KSME Journal, Vol. 10, No. 1, pp. 1~11, 1996

Design Optimization of Hip Prosthesis of Thick Laminated Composites by Developing Finite Element Method and Sensitivity Analysis

Sung Kyu Ha* and Jae Youn Jeong**

(Received October 5, 1994)

An investigation has been performed to develop a finite element method for the analysis of the behavior of complicated three-dimensional thick laminated composite structure, and the method has been applied to the design of hip prosthesis with nonuniform cross-sections. The developed method can accomodate the varying material properties layered within the element and allow the ply-drop-off along the element edges. The numerical results are compared with the analytical solution, and the results show that the number of elements can be reduced up to 80% within 5% error bounds by using the ply-drop-off element. A method of design sensitivity analysis has also been developed to find the optimal ply angles minimizing the deflection of thick laminated composite structures. The developed finited element method together with the design sensitivity analysis has been applied to design of hip stem, and a procedure for calculating the optimum ply angle is proposed to minimize the rotational micromotion which is one of causes of patients' pain.

Key Words : Thick Laminated Composite, Finite Element Analysis, Design Sensitivity Analysis, Hip Prosthesis

Nomenclature

$\boldsymbol{B}$	: Strain-displacement matrix
$\boldsymbol{B}_a$	: Nodal strain-displacement matrix
$\boldsymbol{d}$	: Global displacement vector
$\boldsymbol{d}^e$	: Element nodal displacement vector
E	: Young's Modulus
$\boldsymbol{F}$	: Global force vector
$\boldsymbol{f}^e$	: Element nodal force vector
$\boldsymbol{G}$	: Transformation matrix from global to off-axis coordinates
$\boldsymbol{J}$	: Jacobian matrix of an element
$\boldsymbol{J}^k$	: Jacobian matrix of k-th ply of an element
$\boldsymbol{K}$	: Global stiffness matrix
$\boldsymbol{K}^e$	: Element stiffness matrix
m	: Number of total elements
n	: Number of total plies in an element
N_a	: Isoparametric shape function at node $a(a=1, \cdots\cdots, 8)$
$\boldsymbol{p}$	: Vector of pressure
$\boldsymbol{Q}$	: Stiffness matrix
$\boldsymbol{Q}^k$	: Off-axis stiffness matrix of k-th ply
$\bar{\boldsymbol{Q}}$	: On-axis stiffness matrix
$\boldsymbol{T}$	: Transformation matrix from on-axis to off-axis coordinates
x, y, z	: Cartesian coordinate
x_1, x_2, x_3	: Off-axis cartesian coordinate
$\bar{x}, \bar{y}, \bar{z}$	: On-axis cartesian coordinate
x_a, y_a, z_a	: Cartesian coordinates of node a

Greek Letters

ε^e	: Element strain vector
θ	: Layup angle of each ply
ξ, η, ζ	: Element natural coordinate
ξ^k, η^k, ζ^k	: Sub-natural coordinate
ξ_a, η_a, ζ_a	: Natural coordinate of node
$\xi_a^k, \eta_a^k, \zeta_a^k$	: Sub-natural coordinates of node
$\nu_{xy}, \nu_{yz}, \nu_{zx}$	: Poisson's ratio

* Department of Mechanical Engineering, Hanyang University

** Department of Mechanical Design and Production Engineering, Graduate School, Hanyang University

Superscripts

e	: e-th element
k	: k-th ply number in an element
T	: Transposition of matrix

Subscripts

a	: Node number in an element
b	: Number of design variables
x, y, z	: Cartesian coordinate

1. Introduction

The majority of the patients receiving total hip replacement suffer from serious continuous pain mainly due to the loosening and stress shielding effects leading to femoral failure (Huiskes, 1991; Callagan, et. al., 1992; Crowninshield, et. al., 1981). Those effects result from the micromotion and migration of the hip stem from its original position within the femur. The quest to avoid the implant/bone motion has led to numerous femoral component design variations including alterations in component geometry, consitituent material properties and cementless hip replacement. The study on design features of the hip prosthesis shows that the external geometry, i.e., stem length, component shape and surface texture are extremely crucial to the acute stability of the fixation.

The loosening and stress shielding effects can be adjusted according to the material properties of the hip prosthesis as well as its geometry. Since metallic alloys, i.e., Titanium alloy and Cobalt-Chrome alloy, etc., have been used for the materials, the stiffness of the stem can not be adjusted without changing the geometry. The composite layered hip stem has been thus proposed and widely under investigation mainly because the stiffness can be altered by changing the ply orientations even with the given geometry (Skinner, 1988). In order to determine the ply orientation for the best stiffness, the behavior of the composite hip stem implemented in the femur has to be analyzed.

The finite element analysis (FEA) has been widely used to evaluate the response of the hip stem made of metallic alloy (Huiskes, 1991; Crowninshield, et. al., 1981). The full analysis of the layered composite hip stem using the conventional FEA, however, requires an enormous computing time and memory space since the material properties are varying through the thickness and numbers of elements are, thus, required as many as the ply numbers. Hence, a three-dimensional element for FEA is needed which can handle the varying materials inside the element (Chang, et. al., 1990; Lee, 1980). In addition to that feature, the element should also allow the ply-drop-off along the element edges such that the complicated three-dimensional structure can be accurately modelled. A methodology for FEA is developed, in this study, to analyze the behavior of three-dimensional complicated structures of laminated composites with ply-drop-off on its sides.

An optimization procedure together with the FEA has been also used to obtain better design of the hip stem (Huiskes, 1991; Boeklagen, et. al., 1989). Those investigations are, however, focused mainly on the shape optimization of the metallic alloy. The design sensitivity analysis for the three-dimensional laminated composite structures is now developed for the stiffness optimization to find the optimal ply orientations minimizing the deflection of the structure, and applied to the hip stem for minimization of the circumferential displacement of the total hip prosthesis which is related to the micromotion causing the patients' pain.

2. Statement of the Problem

The total hip prothesis is composed of stem, acrylic cement, cancellous bone, and cortical bone surrounding the stem as shown in Fig. 1. Because the center of gravity of the body is posterior to the axis of the joint, the loads are applied to the head of the stem not only in the frontal plane (in-plane), but also in the sagittal plane (out-of-plane) causing the axial, bending, and torsional effects to the hip prosthesis (Huiskes, 1991; Callaghand, et. al., 1992). The critical micromotion causing the loosening or stress shielding effect is mainly due to the rotational motion

caused by the out-of-plane force acting on the stem head (Fig. 1). The stem is, thus, to have an adequate stiffness to reduce the rotational micromotions. The optimal layup angles are to be determined to obtain the optimal stiffness of composites.

For an optimum design formulation based on the above statement, the circumferential displacement d_y of the total hip prosthesis in the medial-proximal region (A) in Fig. 1 is thus chosen to be

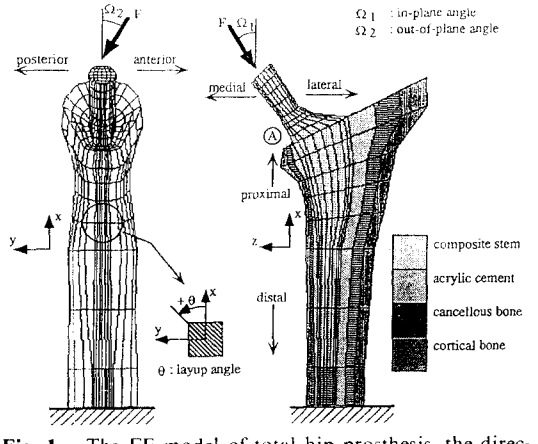

Fig. 1 The FE model of total hip prosthesis, the directions of loading and the constituent materials

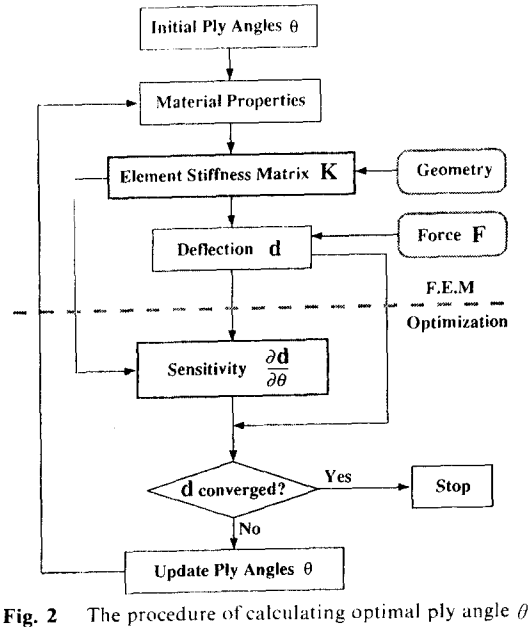

Fig. 2 The procedure of calculating optimal ply angle θ using FEA and optimization

the cost function to be minimized. The ply angles are taken to be the design variables to be found. The formulation for the structural optimum design of the total hip prosthesis is written as follows :

Cost Function : d_y at the medial-proximal interface

Design Variables : $\theta_1, \theta_2, \cdots\cdots, \theta_b$

In oder to find the optimum ply angles, the finite element method which can analyze the thick laminated composites and the design sensitivity analysis are used. The analysis procedure in this study is shown and explained in Fig. 2.

3. Analytical Theory

3.1 Development of multilayered brick element for FEA

A three-dimensional finite element code for the laminated composite structure is developed based on the variational principle. An eight-node, 24 degrees-of-freedom brick element that have the multilayered ply-drop-off along the element edges is developed in order to take care of the variation of the material properties in an element. As will be demonstrated, the element can reduce considerably the amount of memory space and run time required to analyze the three-dimensional behavior of composites.

The three-dimensional displacements $\boldsymbol{d}$ within an element using the eight-node brick element shape functions are expressed as

$$\boldsymbol{d} = \sum_{a=1}^{8} N_a \, \boldsymbol{d}_a \tag{1}$$

where $\boldsymbol{d}_a$ are the nodal displacements which have 3 degrees of freedom (d_x, d_y, d_z) at each node ($a = 1, 2, \cdots\cdots, 8$) as shown in Fig. 3. N_a are the isoparametric shape functions at node a and can be written in the natural coordinates (ξ, η, ζ) as

$$N_1 = \frac{1}{8}(1-\xi)(1-\eta)(1-\zeta)$$

$$N_2 = \frac{1}{8}(1+\xi)(1-\eta)(1-\zeta)$$

$$N_3 = \frac{1}{8}(1+\xi)(1+\eta)(1-\zeta)$$

$$N_4 = \frac{1}{8}(1-\xi)(1+\eta)(1-\zeta)$$

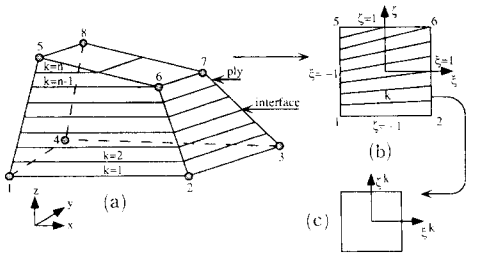

(a) Ply drop-off element and global coordinate system
(b) Lay up sequence in natural coordinate system (ξ, η, ζ)
(c) K-th layer in sub-natural coordinates (ξ^k, η^k, ζ^k)

Fig. 3 Mapping of a multilayered brick element into the natural and sub-natural coordinates for calculation of the element stiffness matrix

$$N_5=\frac{1}{8}(1-\xi)(1-\eta)(1+\zeta)$$
$$N_6=\frac{1}{8}(1+\xi)(1-\eta)(1+\zeta)$$
$$N_7=\frac{1}{8}(1+\xi)(1+\eta)(1+\zeta)$$
$$N_8=\frac{1}{8}(1-\xi)(1+\eta)(1+\zeta) \tag{2}$$

Using the strain-displacement relationship and Eq. (2), the element strain is written as

$$\boldsymbol{\varepsilon}^e=\sum_{a=1}^{8}\boldsymbol{B}_a\,\boldsymbol{d}_a \tag{3}$$

The matrix $\boldsymbol{B}_a$ is defined as

$$\boldsymbol{B}_a=\begin{bmatrix} N_{a,x} & 0 & 0 \\ 0 & N_{a,y} & 0 \\ 0 & 0 & N_{a,z} \\ 0 & N_{a,z} & N_{a,y} \\ N_{a,z} & 0 & N_{a,x} \\ N_{a,y} & N_{a,x} & 0 \end{bmatrix} \tag{4}$$

where a is the nodal number of the element.

Based on the standard finite element procedures as explained by Hughes (1987), the equilibrium equation of the element can be expressed in terms of the nodal desplacements $\boldsymbol{d}^e$ as

$$\boldsymbol{K}^e\,\boldsymbol{d}^e=\boldsymbol{f}^e \tag{5}$$

where $\boldsymbol{f}^e$ is the element nodal force vector. $\boldsymbol{K}^e$ in Eq. (5) is the element stiffness matrix written as

$$\boldsymbol{K}^e=\int_{-1}^{1}\int_{-1}^{1}\int_{-1}^{1}\boldsymbol{B}^T\,\boldsymbol{Q}\,\boldsymbol{B}\,|\,\boldsymbol{J}\,|\,d\xi d\eta d\zeta \tag{6}$$

where the strain-displacement matrix $\boldsymbol{B}$ consists of the matrix $\boldsymbol{B}_a$ in Eq. (4), and $\boldsymbol{Q}$ is the three-dimensional stiffness matrix within the element. The superscript $\boldsymbol{T}$ denotes transposition. $\boldsymbol{J}$ in Eq. (6) is the jacobian matrix defined as

$$\boldsymbol{J}=\begin{bmatrix} x,_\xi & x,_\eta & x,_\zeta \\ y,_\xi & y,_\eta & y,_\zeta \\ z,_\xi & z,_\eta & z,_\zeta \end{bmatrix} \tag{7}$$

To evaluate the determinant of the jacobian matrix, the relationships between the global coordinates (x, y, z) and the natural coordinates (ξ, η, ζ) of the element are used as follows

$$x=\sum_{a=1}^{8}N_a(\xi,\eta,\zeta)x_a$$
$$y=\sum_{a=1}^{8}N_a(\xi,\eta,\zeta)y_a$$
$$z=\sum_{a=1}^{8}N_a(\xi,\eta,\zeta)z_a \tag{8}$$

where x_a, y_a, and z_a are the global coordinates of the node a of the element.

The three-dimensional stiffness matrix $\boldsymbol{Q}$ in Eq. (6) varies within the element as shown in Fig. 3. To account for the variation of the material properties, the element stiffness matrix in Eq. (6) is calculated by separately integrating each layer and summing up all the integrations as follows

$$\boldsymbol{K}^e=\sum_{k=1}^{n}\int_{-1}^{1}\int_{-1}^{1}\int_{-1}^{1}\boldsymbol{B}^T\,\boldsymbol{Q}^k\,\boldsymbol{B}|\,\boldsymbol{J}\,\|\,\boldsymbol{J}^k\,|\,d\xi^k d\eta^k d\zeta^k \tag{9}$$

where k indicates the ply number, and n is the number of the layered plies within the element. $\boldsymbol{Q}^k$ in Eq. (9) is the three-dimensional off-axis stiffness matrix of k-th layer calculated by transforming the on-axis stiffness $\bar{\boldsymbol{Q}}$. The off-axis and

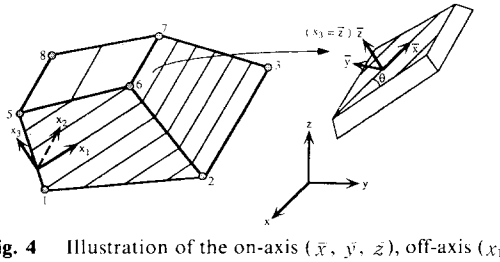

Fig. 4 Illustration of the on-axis ($\bar{x}$, $\bar{y}$, $\bar{z}$), off-axis (x_1, x_2, x_3) and global coordinate system (x, y, z) within a element

on-axis coordinates are illustrated in Fig. 4. The nonzero components of the three-dimensional off-axis stiffness $\boldsymbol{Q}^k$ are derived and shown in terms of $\bar{\boldsymbol{Q}}$ in Appendix and expressed in multiple-angles as following

$$\begin{aligned}
Q_{11} &= U_1 + U_2 \cos 2\theta + U_3 \cos 4\theta \\
Q_{22} &= U_1 - U_2 \cos 2\theta + U_3 \cos 4\theta \\
Q_{12} &= U_4 - U_3 \cos 4\theta \\
Q_{66} &= U_5 - U_3 \cos 4\theta \\
Q_{16} &= \frac{1}{2} U_2 \sin 2\theta + U_3 \sin 4\theta \\
Q_{26} &= \frac{1}{2} U_2 \sin 2\theta - U_3 \sin 4\theta \\
Q_{13} &= U_6 + U_7 \cos 2\theta \\
Q_{23} &= U_6 - U_7 \cos 2\theta \\
Q_{36} &= U_7 \sin 2\theta \\
Q_{44} &= U_8 + U_9 \cos 2\theta \\
Q_{55} &= U_8 - U_9 \cos 2\theta \\
Q_{45} &= -U_9 \sin 2\theta \\
Q_{33} &= U_{10}
\end{aligned} \tag{10}$$

where $U_i (i=1, 2, \cdots\cdots, 10)$ are the linear combinations of on-axis stiffness moduli. The components of U_i and Q_{ij} in Eq. (10) are difined in Appendix. The first 6 equations are the same as those derived by Tsai (1988), As will be shown, the derivatives of Q_{ij} with respect to the ply angle θ are easily performed using Eq. (10).

The region of the k-th layer in the natural coordinates (ξ, η, ζ) is again mapped onto the domain in the sub-natural coordinates (ξ^k, η^k, ζ) as shown in Fig. 3. The new jacobian matrix $\boldsymbol{J}^k$ is defined as

$$\boldsymbol{J}^k = \begin{bmatrix} \xi, _{\xi^k} & \xi, _{\eta^k} & \xi, _{\zeta^k} \\ \eta, _{\xi^k} & \eta, _{\eta^k} & \eta, _{\zeta^k} \\ \zeta, _{\xi^k} & \zeta, _{\eta^k} & \zeta, _{\zeta^k} \end{bmatrix} \tag{11}$$

To evaluate the jacobian matrix in Eq. (11), the relationships between the natural coordinates (ξ, η, ζ) of the element and the k-th sub-natural coordinates (ξ^k, η^k, ζ^k) are used, i.e.,

$$\begin{aligned}
\xi &= \sum_{a=1}^{8} N_a(\xi^k, \eta^k, \zeta^k)\xi_a^k \\
\eta &= \sum_{a=1}^{8} N_a(\xi^k, \eta^k, \zeta^k)\eta_a^k \\
\zeta &= \sum_{a=1}^{8} N_a(\zeta^k, \eta^k, \zeta^k)\zeta_a^k
\end{aligned} \tag{12}$$

Where ξ_a^k, η_a^k, and ζ_a^k are the coordinates of the corner a of k-th layer in the natural coordinate system (Fig. 3), and N_a are the shape functions defined in Eq. (2). When the nodes 1, 2, 3, and 4, and the nodes 5, 6, 7, and 8 are located in the same ply interfaces, respectively, the element has no ply-drop-offs on top and bottom surfaces and the determinant of $\boldsymbol{J}^k$ in Eq. (11) is reduced to t^k/h as proposed by Lee (1980) and Chang, et. al., (1990) where t^k is the thickness of k-th ply and h is the total thickness of the element.

As shown in Eq. (12), in order to evaluate the element stiffness matrix $\boldsymbol{K}^e$ in Eq. (9), the coordinates ξ_a^k, η_a^k, and ζ_a^k are needed in addition to the conventional data, i.e., the nodal coordinates, element connectivities and material properties. After conventional mesh generation, the ply interface numbers where the nodes are located are automatically calculated in this study using the data of the layup sequence ; at each node, the normal distance is calculated from the node to the reference suface which is represented by the first ply. Using the ply interface number of each node, the number of layered plies n within each element and the coordinates of the corner a of k-th layer ξ_a^k, η_a^k, ζ_a^k, and the determinant of $\boldsymbol{J}^k$ are can be automatically calculated.

3.2 Design sensitivity analysis

The sensitivity of the cost function (displacement in this study) with respect to the design variables θ_i can be calculated using the global equilibrium equation expressed in terms of displacements which is obtained through the finite element formulation from the element stiffness matrix and force vector in Eq. (5), i.e.,

$$\boldsymbol{K}\boldsymbol{d} = \boldsymbol{F} \tag{13}$$

where $\boldsymbol{d}$ is the global displacement vector, and $\boldsymbol{K}$ and $\boldsymbol{F}$ are the global stiffness matrix and force vector, respectively. In Eq. (13), the global stiffness matrix $\boldsymbol{K}$ is expressed by the element stiffness matrix $\boldsymbol{K}^e$ and the transformation matrix $\boldsymbol{G}^e$ from global to off-axis(element) coordinates shown in Fig. 4.

$$\boldsymbol{K} = \sum_{e=1}^{m} (\boldsymbol{G}^e)^T \boldsymbol{K}^e \boldsymbol{G}^e \tag{14}$$

m in Eq. (14) indicates the number of the total

elements.

The derivative of the displacement $\boldsymbol{d}$ with respecct to the design variables $\theta^k(i=1, 2, \cdots\cdots, b)$ are calculated using Eq. (13) where $\boldsymbol{F}$ is independent of θ_i, i, e.,

$$\frac{\partial \boldsymbol{d}}{\partial \theta_i} = -\boldsymbol{K}^{-1} \frac{\partial \boldsymbol{K}}{\partial \theta_i} \boldsymbol{d} \tag{15}$$

In order to evaluate Eq. (15), in each step of optimization, the displacement $\boldsymbol{d}$ and stiffness matrix $\boldsymbol{K}$ are calculated by solving Eq. (13). The derivative of the stiffness with respect to the design variables θ_i in Eq. (15) are calculated using Eq. (9) and Eq. (14) where $\boldsymbol{G}^e$ is independent of θ_i i.e.,

$$\frac{\partial \boldsymbol{K}}{\partial \theta_i} = \sum_{e=1}^{m} (\boldsymbol{G}^e)^T \frac{\partial \boldsymbol{K}^e}{\partial \theta_i} \boldsymbol{G}^e$$
$$= \sum_{e=1}^{m} (\boldsymbol{G}^e)^T \sum_{k=1}^{n} \int_{-1}^{1}\int_{-1}^{1}\int_{-1}^{1} \boldsymbol{B}^T \frac{\partial \boldsymbol{Q}^k}{\partial \theta_i} \boldsymbol{B} \,|\boldsymbol{J}|\, |\boldsymbol{J}^k| \, d\xi^k d\eta^k d\zeta \, \boldsymbol{G}^e \tag{16}$$

Since Eq. (16) is the same as the global stiffness matrix $\boldsymbol{K}$ with $\boldsymbol{Q}^k$ replaced with $\partial \boldsymbol{Q}^k / \partial \theta_i$ in the element stiffness matrix, the assembly of the element matrix in Eq. (16), hence, use the same procedure as the conventional finite element method. Using the transformation of the stiffness matrix expressed in multiple-angles in Eq. (10), where U_i are independent of the ply angle θ_i, $\partial \boldsymbol{Q}^k / \partial \theta_i$ in Eq. (16) can be calculated and expressed in terms of the off-axis stiffness $\boldsymbol{Q}^k$.

$$\begin{aligned}
Q'_{11} &= -4Q_{16} \\
Q'_{22} &= 4Q_{26} \\
Q'_{12} &= 2(Q_{16} - Q_{26}) \\
Q'_{66} &= 2(Q_{16} - Q_{26}) \\
Q'_{16} &= Q_{11} - Q_{12} - 2Q_{66} \\
Q'_{26} &= -Q_{22} + Q_{12} + 2Q_{66} \\
Q'_{13} &= -2Q_{36} \\
Q'_{23} &= 2Q_{36} \\
Q'_{36} &= Q_{13} - Q_{23} \\
Q'_{44} &= 2Q_{45} \\
Q'_{55} &= -2Q_{45} \\
Q'_{45} &= Q_{55} - Q_{44} \\
Q'_{33} &= 0
\end{aligned} \tag{17}$$

In Eq. (17), the prime indicates the derivative of $\boldsymbol{Q}^k$ with respect to θ_i.

4. Numerical Verification of the Analysis

4.1 Verification of finite element code

A three-dimensional finite element program "HUSAP" with pre- and post-processor is developed based on the theory presented in Sec. 3. In order to verify the finite element code and analysis, calculations were performed and compared with the existing analytical solutions.

As a verification, the deflections and stresses of 0.1m long and 0.002m wide angle ply $[0/90]_n$

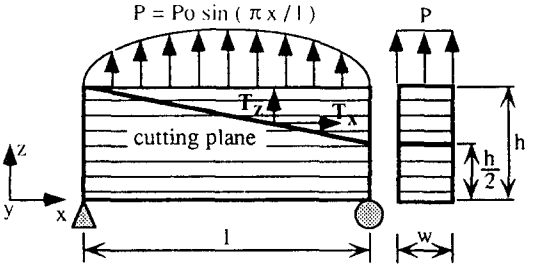

(a) Calculation of the tractions along the cutting plane in the angle ply $[0/90]_{40}$ laminate

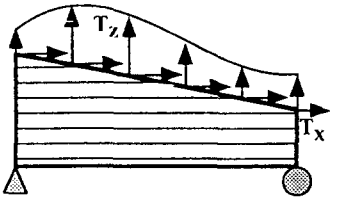

(b) Ply drop-off model subjected to the tractions along the cutting plane

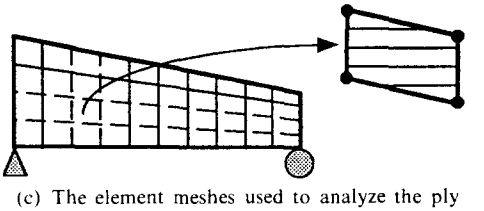

(c) The element meshes used to analyze the ply drop-off model

Fig. 5 Verification model for ply-drop-off element
l=0.1 m w=0.002 m h=0.0102 m
ply thickness=0.000127 m P_o=1.0 N

laminate are calculated. The laminate is subjected to pressure $p(x, y)=p_0 \sin \frac{\pi}{l} x$ on the top surface and simply supported at the ends as shown in Fig. 5(a). The number of sub-laminate n is chosen to be 40, i.e., 80 plies total. The exact solutions of displacements and stresses can be obtained using the method presented by Pagano (1969). In order to consider the ply-drop-off, a structure which has a cutting plane is analyzed as shown in Fig. 5(b). It has 40 plies in the right side. The applied loads on the top surface were calculated from the above exact solution along the corresponding cutting plane. Hence, the displacements and stresses of the structure with the cutting plane are the same as the above exact solution of the structure without the cutting plane. Three different element numbers, i.e., 40 (case 1), 10 (case 2) and 5 (case 3) are considered through the thickness for FEA using the ply-drop-off elements. The considered numbers of elements in x and y-direction are 20 and 1, respectively. The displacement d_z and stress σ_x at the bottom surface are calculated and compared with the exact solution as shown in Fig. 6. The required node numbers, computing time and accuracy for each case are also summarized in Table 1.

As shown in Fig. 6, and Table 1, the calculated

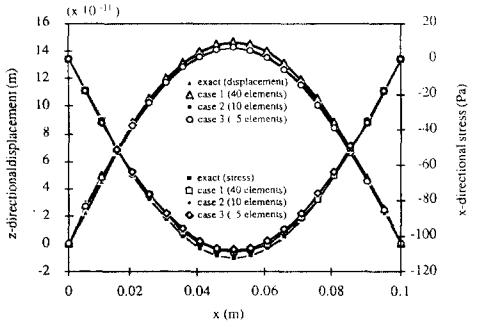

Fig. 6 Comparision of the numerical calculations and the exact solutions

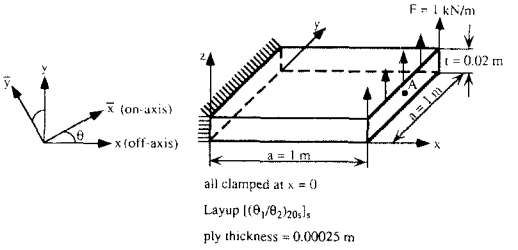

(a) Cantilevered plate subjected to the uniformly distributed end loads

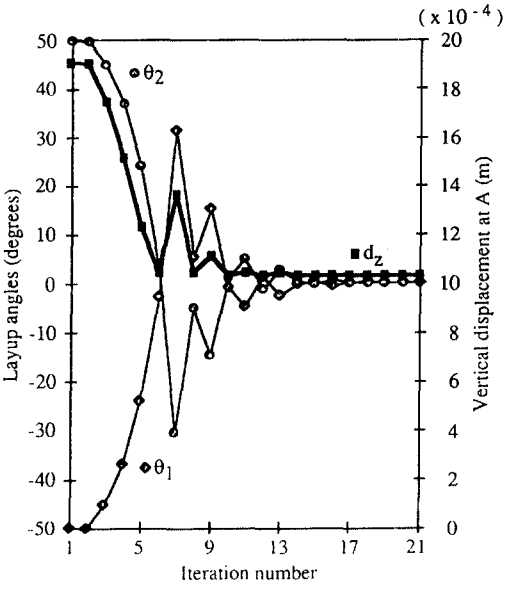

(b) The value of vertical displacement d_z and ply angles θ_1, θ_2 with respect to the iteration numbers

Fig. 7 Verification model and numerical results for design sensitivity analysis

Table 1 Comparision of the numerical caculations and the exact solutions

case no.	no. of nodes	no. of elements	C. P. U. time of PC-486 (min : sec)	max. displacement		max. stress	
				value	error	value	error
exact				1.5E-10		-112.5	
case 1	1722	800	2 : 05.94	1.5E-10	0.49%	-109	3.12%
case 2	462	200	1 : 07. 40	1.4E-10	2.51%	-108	4.01%
case 3	252	100	1 : 10.09	1.4E-10	2.79%	-108	4.01%

Table 2 Material properties of stem, cement and bone components

Material property	unit	T300/976 (Graphite/Epoxy)	Acrylic cement	Cancellous bone	Cortical bone
Exx	GPa	176.00	2.07	0.3246	17.00
Eyy=Ezz	GPa	11.10	2.07	0.3246	17.00
Exy=Exz	GPa	7.65	0.90	0.1258	3.28
Eyz	GPa	4.27	0.90	0.1258	3.64
Vxy=Vxz		0.3	0.19	0.29	0.46
Vyz		0.3	0.19	0.29	0.58

displacements and stresses using the multi-layered ply-drop-off element are matching very well with the exact solution. In addition, node numbers or computing memory can be significantly saved without sacrificing the accuracy by using the ply-drop-off elements.

4.2 Verification of design sensitivity analysis

In order to verify the design sensitivity analysis, the optimal ply angles of the cantilevered laminated plate are searched using the verified finite element code and the design sensitivity analysis. The initial layup is taken as $[(-50/50)_{20s}]_s$, and the ply thickness is 0.00025m. The plate is clamped at $x=0$ and subjected to the uniformly distributed and loads $F=1$kN/m as shown in Fig. 7(a), and the material properties of the composites (T300/976) are shown in Table 2. The cost function is the z-directional displacements at the center of the free end.

As a result, the values of design variables θ_1, θ_2 and the cost function d_z are obtained and plotted with respect to the iteration as shown Fig. 7(b). The values of θ_1 and θ_2 are, as expected, converged to zero degrees after about 20 iterations.

5. Results and Discussion

A numerical calculation is performed using the developed finite element program together with the optimization module developed by Vanderplaats, 1985, where the design sensitivity is carried out using Eqs.(13)~(17).

The total hip prosthesis of length 0.193m is considered and the generated finite element meshes are shown in Fig. 1. The numbers of generated nodes and elements are 1827 and 1440, respectively. The node for minimizing the circumferential displacement is selected at medial-proximal interface between stem and cement as indicated (A) in Fig. 1. The composite material used for the hip stem in this study is Graphite/Epoxy Fiberite T300/976, and its material properties are shown in Table 2. The layup sequence is chosen to be $[(\theta_1/\theta_2)_{ns}]_s$, where two independent ply angles are considered and n indicates the number of ply group. Acrylic cement and cancellous bone are isotropic, and cortical bone is assumed to the transversely isotropic as studied in Huiskes (1991), Crowninshield, et. al. (1981) and Vichnin, et. al. (1986). The material properties of these cement and bone components are also shown in Tale 2. The contact forces acting on the head during the gait are ranging from 3 to 5 times the body weight (Huiskes, 1991). As reported by Crowninshield, et. al. (1981) and Davy, et. al. (1988) in-plane and out-of-plane angles of the force are ranging from 10 to 20 degrees and 0 to 35 degrees, respectively (Fig. 1). For a numerical calculation, a force of 1,620 N corresponding to 3 times of 55kg person is, hence, applied to hip stem model with in-plane angle 15 degrees and out-of-plane angle 5 degrees, respectively (Fig. 1).

The optimum ply angle is calculated using the procedure explained in Fig. 2 with the initial layup sequence $[(15/15)_{3s}]_s$. The calculated values of circumferential displacement d_y and ply angles θ_1, θ_2 with respect to the iteration numbers are shown in Fig. 8. The minimum circumferen-

tial displacement and corresponding layup angles are obtained as 1.98×10^{-4}m and -29.0, -31.0 degrees, respectively, at a iteration number 18 (Fig. 8). The optimal layup sequence in this study to minimize the micromotions between stem and bone can thus be written as $[(-29/-31)_{35s}]_s$ of the total hip prosthesis considered. The deflection curve of the layup sequences $[(-29/-31)_{35s}]_s$ is compared with other layup sequences $[(29/-31)_{35s}]_s$ and $[(29/31)_{35s}]_s$ as shown in Fig. 9.

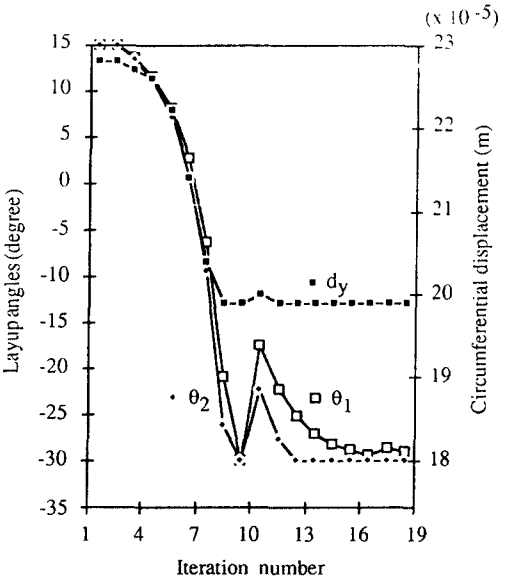

Fig. 8 The values of circumferential displacement d_y and ply angles θ_1, θ_2 with respect to the iteration numbers

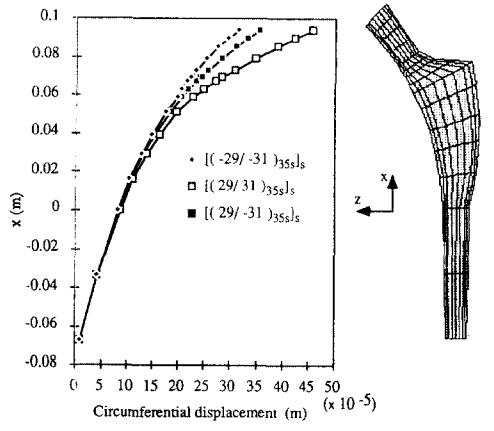

Fig. 9 Comparison of the circumferential displacements d_y of 3 different layups

The result shows that the circumferential deflection of the composite hip stem subjected to not only the vertical force but also the circumferential force can be minimized using the unbalanced layup sequence. In other words, the positive deflection due to the circumferential component of the force is offset by the negative deflection caused by the unbalanced laminate subejcted to the vertical component of the force. In this study, the optimal ply angles of $[(\theta_1/\theta_2)_{ns}]_s$ are searched in order to minimize the displacement, but the different optimal ply angles could be obtained with the different angle sequences. The methods for the shape and strength optimization as well as the stiffness optimization can be also developed for the three-dimensional structure of the laminated composite materials. Most importantly, strength as well as the displacement of the structure can be also either a cost function or a constraint function. The disign sensitivity analysis developed in this study should be then extended to include the sensitivity of the stresses with respect to the ply angles.

Reference

Callaghan, J. J., Fulghum, C. S., Glisson, R. R. and Stranne, S. K., 1992, "The Effect of Femoral Stem Geometry on Interface Motion in Uncemented Porous-Coated Total Hip Prostheses," *Journal of Bone and Joint Surgery*, Vol. 74-A, No. 6, pp. 839~848.

Chang, F. K., Perez, J. L. and Chang, K. Y., 1990, "Analysis of Thick Laminated Composites," *Journal of Composite Materials*, Vol. 24, No. 8, pp. 801~822.

Crowninshield, R. D. Brand, R. A., Johnston, R. C. and Pederson, D. R., 1981, "An Analysis of Collar Function and the Use of Titanium in Femoral Prostheses," *Clinical Orthopaedics and Related Research*, No. 158, pp. 270~277.

Davy, D. T., Kotzar, G. M., Brown, R. H., Heiple, K. G., Goldberg, V. M. Heiple, K. G. Jr., Berills, J. and Burstein, A. H., 1988, "Telemetric Force Measurements across the Hip after Total

Arthroplasty," *Journal of Bone and Joint Surgery*, Vol. 70-A, No. 1, pp. 45~50.

Hughes, T. J. R., 1987, *The Finite Element Method*, Prentice-Hall, New Jersey.

Huiskes, R., 1991, "Biomechanics of Artificial-Joint Fixation," *Basic Orthopaedic Biomechanics*, Raven Press., New York.

Huiskes, R. and Boeklagen, R., 1989, "Mathematical Shape Optimization of Hip Prosthesis Design," *Journal of Biomechanics*, Vol. 22, No. 8/9, pp. 793~804.

Lee. J. D., 1980, "Three Dimensional Finite Element Analysis of Layered Fiber-Reinforced Composite Matetrials," *Computers and Structures*, No. 12, pp. 319~339.

Pagano, N. J., 1969, "Exact Solutions for Composite Laminates in Cylindrical Bending," *Journal of Composite Materials*, Vol. 3, pp. 398~409.

Skinner, H. B., 1988, "Composite Technology for Total Hip Arthroplasty," *Clinical Orthopaedics and Related Research*, No. 235, pp. 224~236.

Tsai, S. W., 1988, *Composites Design*, Fourth Edition, Think Composities, Dayton, U. S. A.

Vanderplaats, G. N., 1985, "ADS- A Fortran Program for Automated Design Synthesis."

Vichin, H. H. and Batterman, S. C., 1986, "Stress Analysis and Failure Prediction in the proximal Femur Before and After Total Hip Replacement," *Journal of Biomechanical Eng.*, Vol. 108, pp. 33~41.

APPENDIX : Transformation of the Stiffness Matrix Q

The off-axis stresses can be expressed in compact matrix form using symmetry of stresses and contracted notation.

$$[\sigma]=\begin{bmatrix}\sigma_{11} & \sigma_{12} & \sigma_{13}\\ \sigma_{21} & \sigma_{22} & \sigma_{23}\\ \sigma_{31} & \sigma_{32} & \sigma_{33}\end{bmatrix}=\begin{bmatrix}\sigma_1 & \sigma_6 & \sigma_5\\ \sigma_6 & \sigma_2 & \sigma_4\\ \sigma_5 & \sigma_4 & \sigma_3\end{bmatrix} \tag{A1}$$

The contracted stress matrix in Eq. (A1) is arranged as a column vector

$$\{\sigma\}=\{\sigma_1\ \sigma_2\ \sigma_3\ \sigma_4\ \sigma_5\ \sigma_6\}^T \tag{A2}$$

and the off-axis strains can be also expressed using a contracted notation

$$\begin{aligned}\{\varepsilon\}&=\{\varepsilon_{11}\ \varepsilon_{12}\ \varepsilon_{33}\ 2\varepsilon_{23}\ 2\varepsilon_{13}\ 2\varepsilon_{12}\}^T\\ &=\{\varepsilon_1\ \varepsilon_2\ \varepsilon_3\ \varepsilon_4\ \varepsilon_5\ \varepsilon_6\}^T\end{aligned} \tag{A3}$$

The relationship between stresses and strains are expressed as following

$$\begin{Bmatrix}\sigma_1\\ \sigma_2\\ \sigma_3\\ \sigma_4\\ \sigma_5\\ \sigma_6\end{Bmatrix}=\begin{bmatrix}Q_{11} & Q_{12} & Q_{13} & 0 & 0 & Q_{16}\\ Q_{21} & Q_{22} & Q_{23} & 0 & 0 & Q_{26}\\ Q_{31} & Q_{32} & Q_{33} & 0 & 0 & Q_{36}\\ 0 & 0 & 0 & Q_{44} & Q_{45} & 0\\ 0 & 0 & 0 & Q_{54} & Q_{55} & 0\\ Q_{61} & Q_{62} & Q_{63} & 0 & 0 & Q_{66}\end{bmatrix}\begin{Bmatrix}\varepsilon_1\\ \varepsilon_2\\ \varepsilon_3\\ \varepsilon_4\\ \varepsilon_5\\ \varepsilon_6\end{Bmatrix} \tag{A4}$$

where Q_{ij} is obtained by transforming the on-axis stiffness $\bar{Q}_{ij}$. Using s for sin θ and c for cos θ, the components of the off-axis stiffness Q_{ij} are

$$\begin{aligned}
Q_{11}&=s^4\overline{Q_{22}}+c^4\overline{Q_{11}}+2s^2c^2(\overline{Q_{12}}+2\overline{Q_{66}})\\
Q_{22}&=s^4\overline{Q_{11}}+c^4\overline{Q_{22}}+2s^2c^2(\overline{Q_{12}}+2\overline{Q_{66}})\\
Q_{12}&=(s^4+c^4)\overline{Q_{12}}+s^2c^2(\overline{Q_{11}}+\overline{Q_{22}}-4\overline{Q_{66}})\\
Q_{66}&=(c^2-s^2)^2\overline{Q_{66}}+c^2s^2(\overline{Q_{11}}-2\overline{Q_{12}}+\overline{Q_{22}})\\
Q_{16}&=s^3c(\overline{Q_{12}}-\overline{Q_{22}}+2\overline{Q_{66}})\\
&\quad+c^3s(\overline{Q_{11}}-\overline{Q_{12}}-2\overline{Q_{66}})\\
Q_{26}&=s^3c(\overline{Q_{11}}-\overline{Q_{12}}-2\overline{Q_{66}})\\
&\quad+c^3s(\overline{Q_{12}}-\overline{Q_{22}}+2\overline{Q_{66}})\\
Q_{13}&=s^2\overline{Q_{23}}+c^2\overline{Q_{13}}\\
Q_{23}&=s^2\overline{Q_{13}}+c^2\overline{Q_{23}}\\
Q_{36}&=cs(\overline{Q_{13}}-\overline{Q_{23}})\\
Q_{44}&=c^2\overline{Q_{44}}+s^2\overline{Q_{55}}\\
Q_{55}&=s^2\overline{Q_{44}}+c^2\overline{Q_{55}}\\
Q_{45}&=cs(\overline{Q_{55}}-\overline{Q_{44}})\\
Q_{33}&=\overline{Q_{33}}
\end{aligned} \tag{A5}$$

Eq. (A5) is expressed in multi-angles as in Eq. (10) where U_i are defined as

$$\begin{aligned}
U_1&=\frac{3}{8}\overline{Q_{11}}+\frac{3}{8}\overline{Q_{22}}+\frac{1}{4}\overline{Q_{12}}+\frac{1}{2}\overline{Q_{66}}\\
U_2&=\frac{1}{2}\overline{Q_{11}}-\frac{1}{2}\overline{Q_{22}}\\
U_3&=\frac{1}{8}\overline{Q_{11}}+\frac{1}{8}\overline{Q_{22}}-\frac{1}{4}\overline{Q_{12}}-\frac{1}{2}\overline{Q_{66}}\\
U_4&=\frac{1}{8}\overline{Q_{11}}+\frac{1}{8}\overline{Q_{22}}+\frac{3}{4}\overline{Q_{12}}-\frac{1}{2}\overline{Q_{66}}\\
U_5&=\frac{1}{8}\overline{Q_{11}}+\frac{1}{8}\overline{Q_{22}}-\frac{1}{4}\overline{Q_{12}}+\frac{1}{2}\overline{Q_{66}}\\
U_6&=\frac{1}{2}\overline{Q_{13}}+\frac{1}{2}\overline{Q_{23}}
\end{aligned}$$

$$U_7=\frac{1}{2}\overline{Q_{13}}-\frac{1}{2}\overline{Q_{23}} \qquad U_9=\frac{1}{2}\overline{Q_{44}}-\frac{1}{2}\overline{Q_{55}}$$

$$U_8=\frac{1}{2}\overline{Q_{44}}+\frac{1}{2}\overline{Q_{55}} \qquad U_{10}=\overline{Q_{33}} \qquad \text{(A6)}$$